Received: 8 September 2021 | Accepted: 28 September 2021

DOI: 10.1002/bab.2267

ORIGINAL ARTICLE

WILEY

Identifying mineral decrement with bone injury by quantifying osteocalcin on current-volt sensor

Huanjie Bi[1] | **Peimin Bian**[2] | **Subash C. B. Gopinath**[3,4] | **Kasi Marimuthu**[5] | **Genbing Lv**[6] | **XinHua Yin**[7]

[1] The Second Department of Orthopedics, Tangshan Gongren Hospital, Tangshan, Hebei, China

[2] Department of Medical Rehabilitation, The 5th People's Hospital of Jinan, Jinan, Shandong, China

[3] Faculty of Chemical Engineering Technology, Universiti Malaysia Perlis (UniMAP), Arau, Perlis 02600, Malaysia

[4] Institute of Nano Electronic Engineering, Universiti Malaysia Perlis (UniMAP), Kangar, Perlis 01000, Malaysia

[5] Department of Biotechnology, Faculty of Applied Sciences, AIMST University, Bedong, Kedah, Malaysia

[6] Department of Orthopedics, Sun Si Miao Hospital of Beijing University of Chinese Medicine, Tongchuan Traditional Chinese Medicine Hospital, Tongchuan, Shaanxi, China

[7] Department of Spine Surgery, HongHui Hospital, Xi'an Jiaotong University College of Medicine, Xi'an, Shaanxi, China

Correspondence
Genbing Lv, Department of Orthopedics, Sun Si Miao Hospital of Beijing University of Chinese Medicine, Tongchuan Traditional Chinese Medicine Hospital, Tongchuan, Shaanxi 727031, China.
Email: 13325397833@sina.cn
XinHua Yin, Department of Spine Surgery, HongHui Hospital, Xi'an Jiaotong University College of Medicine, No. 76 Nanguo Rd, Beilin District, Xi'an, Shaanxi 710054, China.
Email: mangiferia@sina.com

Abstract

Osteoporosis, a bone disease is caused by the deterioration of bone and shows an enhanced risk of bone fracture and decreasing bone mineral density. Unfortunately, the available radiological techniques are expensive, and have disadvantages such as radiation intake, need a specialist to handle the instrument, and so forth. This research is focused to develop a point-of-care system to identify osteocalcin on current-volt sensor, which helps to diagnose the bone metabolism and prognostics. Antiosteocalcin antibody was attached on the electrode through the silane-modified iron material. The antibody-immobilized sensing surface was utilized to identify the level of osteocalcin and the detection limit of 100 pg/ml reached on linear concentrations of 0.01–3000 ng/ml. Calculations were made by triplicates ($n = 3$; 3δ) on the determination coefficient of $y = 0.2637x–0.6012$; $R^2 = 0.9319$. Further, control proteins failed to bind with immobilized antibody, confirmed by the specific osteocalcin detection. This research is to identify the osteoporosis biomarker and to help determine the conditions with osteoporosis.

KEYWORDS
biomarker, biosensor, iron oxide material, osteoporosis

Abbreviations: IDE, Interdigitated electrode; APTMS, (3-Aminopropyl)triethoxysilane; NaOH, Sodium hydroxide; H_2SO_4, Sulfuric acid; PEG-COOH, Polyethylene Glycol Carboxyl; IOM, Iron oxide material; h, Hour; FESEM, Field-emission Scanning Electron Microscope; EDX, Energy Dispersive X-Ray Analysis; RCA, Radio Corporation of America; Al, Aluminum; UV, Ultraviolet; PBS, Phosphate-buffered saline; V, Volt

1 | INTRODUCTION

Osteoporosis is a bone disease, caused by the deterioration of bone tissue, leads to weakening of bone density, which can ultimately lead to bone fracture.[1–3] In general, healthy bones have the structure of honey bomb, and under the condition with osteoporosis, the spaces and holes in the honeycomb become much larger, which causes the loss in mass and density (Figure 1A,B).[1] As a result, the less dense bone becomes weaker and likely to break even by a simple movement. There are various poor lifestyle habits, such as consumption of junk food and alcohol, lack of vitamin D, and less physical activities, which mainly influence the bone weakening.[4,5] Because one cannot feel easily the bone weakening or bone loss, osteoporosis is named as a silent disease until the bone fracture occurs. Sometimes it is difficult to differentiate between osteoporosis, osteosarcoma, and arthritis due to the very similar symptoms.[6,7] To avoid such a situation, early and specific prediction of bone-related issues is mandatory. Various methods and techniques are developed by the researchers to monitor the health issues by quantifying the blood-based biomarkers.[1,2,8–11] Osteocalcin is the bone gamma-carboxyglutamic acid containing protein that is released from osteoblasts during the process of bone formation.[12,13] In general, a patient with osteoporosis has deficiency of phosphorus and calcium levels, the calcium-dependent biomarker "osteocalcin" is responsible for bone mineralization. In addition, osteoporosis decreases the formation of hydroxyapatite, which causes the increase in the level of osteocalcin in blood serum.[14] So, quantifying osteocalcin level helps to identify the condition of the bone and for giving a proper treatment before the bone-fracturing condition. In this research, osteocalcin biosensor is developed on iron oxide material (IOM)-modified interdigitated electrode current-volt sensor.

Metallic applications are widely agreed in the biosensor field to elevate the analyte–ligand interaction. Nanomaterials are synthesized with various sizes and shapes and utilized for sensing surface functionalization.[15–19] Gold, graphene, silver, aluminum, tungsten, zinc, cobalt, and iron are the common materials used for various medical applications including surface preparation and to conjugate with biomolecules to improve the detection.[20–25] In addition, nanomaterials are applied efficiently in the field of orthopedic applications.[26] Various researches have proven that nanomaterial-conjugated probes or analyte molecules are more stable on the sensor surfaces and give a proper orientation for the biomolecules, which improves the ligand–analyte interaction. Iron material brings out positive features such as high surface area to volume ratio and improves electron transfer between the biomolecule and electrode. Herein, IOM extracted from the coal fly ash was used for the antibody attachment on

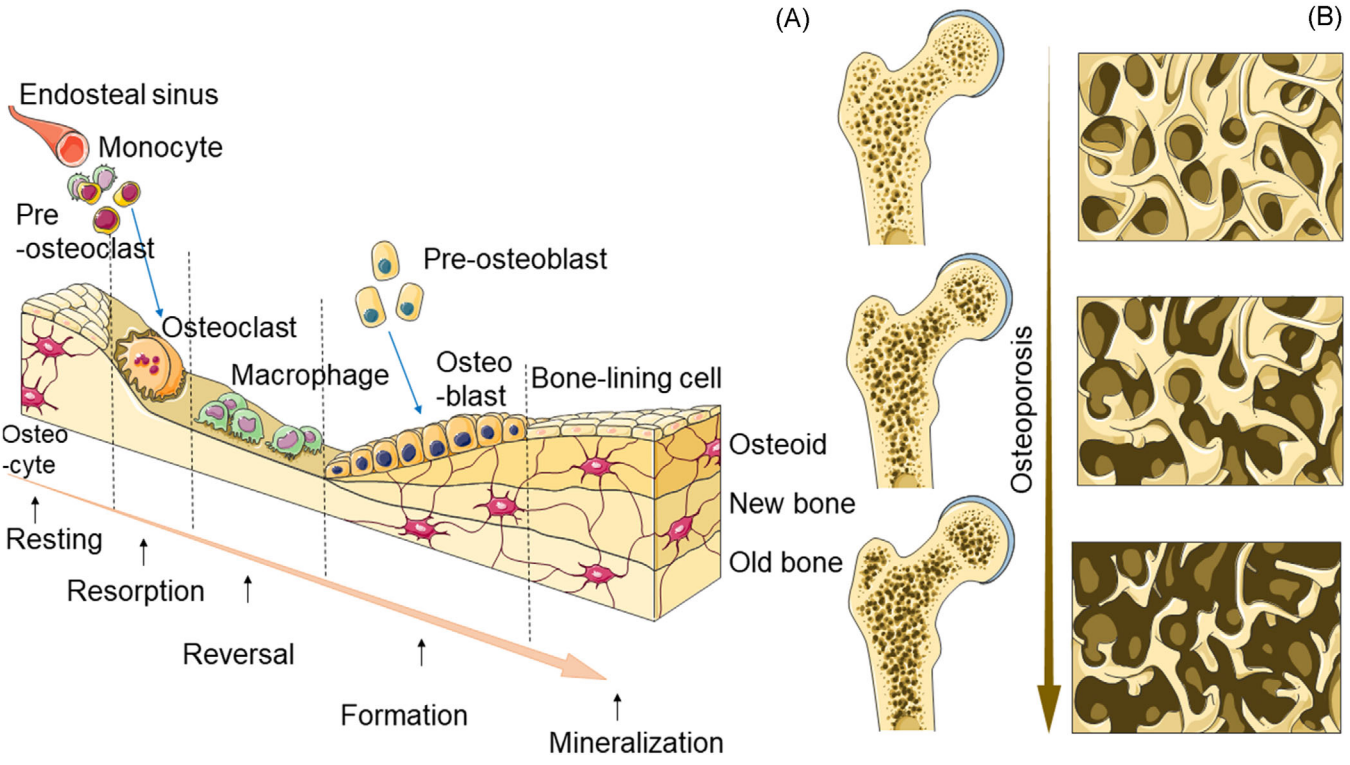

FIGURE 1 Correlation of osteocalcin and osteoporosis. (A) Remodeling process of bone. (B) Changes in bone with osteoporosis. The bottom long arrow indicates the development of osteoporosis

the interdigitated electrode (IDE) surface, which helps to attract higher numbers of probe with the ultimate interaction with osteocalcin and increases the current response.

IDE is one of the most established transducing surfaces, widely used in various fields, especially for chemical and biological sensing due to its highly sensitive, convenient fabrication process and it being inexpensive.[27,28] This sensor operates by the dipole moment between positive and negative electrodes due to the electronegativity of two atoms on the sensing surface. In this study, silane-modified iron material was attached on IDE sensing electrode surface and then antiosteocalcin was attached through amine and carboxylic interaction. The antibody-immobilized electrode surface was utilized to quantify the osteocalcin level, and thus helps to identify the osteoporosis condition.

2 | MATERIALS AND METHODS

2.1 | Molecules

(3-Aminopropyl)triethoxysilane (APTMS), sodium hydroxide (NaOH), sulfuric acid (H_2SO_4), osteocalcin, antiosteocalcin antibody, and PEG-COOH were purchased from Sigma Aldrich (MO, USA). Whatman filter paper and ethanol were received from Thermo Fisher Scientific (MA, USA). Current-volt measurements were done by Keithley 6487 Picoammeter (voltage/current).

2.2 | IOM preparation from fly ash

IOM was prepared from the waste product of coal mine fly ash. For this process, initially iron mixed in the fly ash was separated. A 100 g fly ash was suspended in 500 ml of distilled water and placed on a magnetic stirrer and stirred for 20 min. In this process, the iron material was stacked on the magnetic rod and it was collected. This process was continued until all the iron material from the fly ash was collected. The separated iron was washed by distilled water several times until it was pure, and then it was made to dry under room temperature. Further, 5 g of collected iron was mixed with 500 ml of sulfuric acid (20%) and stirred for 3 h (at 50°C). And then, the iron-dissolved solution was filtered by Whatman filter paper, and the residue was discarded. The extracted iron-containing solution (at acetic pH) was placed on a stirrer, and then 20 nM of diluted sodium hydroxide was added slowly until the solution reached the neutral pH. At this stage, a clear orange color gel was formed, the gel was placed in the stirrer for 18 h to get the uniform-sized material. After 18 h, the gel was separated by centrifugation, and then washed with distilled water many times. Finally, the obtained gel was dried in the oven at 120°C (for 1 h) to get the powder form of iron material. The imaging of the obtained nanoparticle was analyzed by FESEM analysis, and the elements in the material were confirmed with EDX analysis.

2.3 | Electrode surface fabrication

Initially, the desired gap size, length, and thickness of the electrode was drawn with the AutoCAD software and then transferred on the photomask. Fabrication and transformation processed were involved in the following procedures: (a) Si wafer was cleaned by RCA1 and RCA2; (b) at 500°C, thermal oxidation was conducted (for 1 h) to create the layer of SiO_2; (c) Al layer was deposited with thermal evaporator and Al coil; (d) spin coater was utilized to coat the positive photoresist; (e) pattern was transferred on the photoresist by using UV-light exposure; (f) electrode surface was dipped in the photoresist developer and Al etching solution was used to clear the unexposed area; and (g) electrode was washed with acetone and distilled water.

2.4 | Amine modification on IOM

Amine modification was carried out on IOM to create a linker between the electrode surface and the antibody. Silane coupling with APTMS was carried out to create the amine liner on IOM. For this process, 1% of APTMS was mixed with 1 g of synthesized IOM and heated at 150°C overnight under the stirring condition. Then the silane-modified IOM was separated by centrifugation for 15 min at 10,000 rpm. The surface of IOM was washed with diluted ethanol many times to remove the unbound APTMS, and the finally obtained product was dried in the oven at 120°C (for 1 h) to get the powder form of modified iron material.

2.5 | Sensing surface preparation for antibody immobilization

Antibody was attached on the electrode surface by using silane-modified IOM as the connector. Initially, the surface was dipped in 1% of potassium hydroxide (for 10 min) and then the surface was washed thoroughly with distilled water. Further, 1 g of APTMS-modified IOM diluted in ethanol was dropped on the electrode surface and rested (for 3 h). And then the electrode surface was washed with ethanol to remove the unbound APTMS. Finally, 200 nM of antiosteocalcin antibody was dropped on

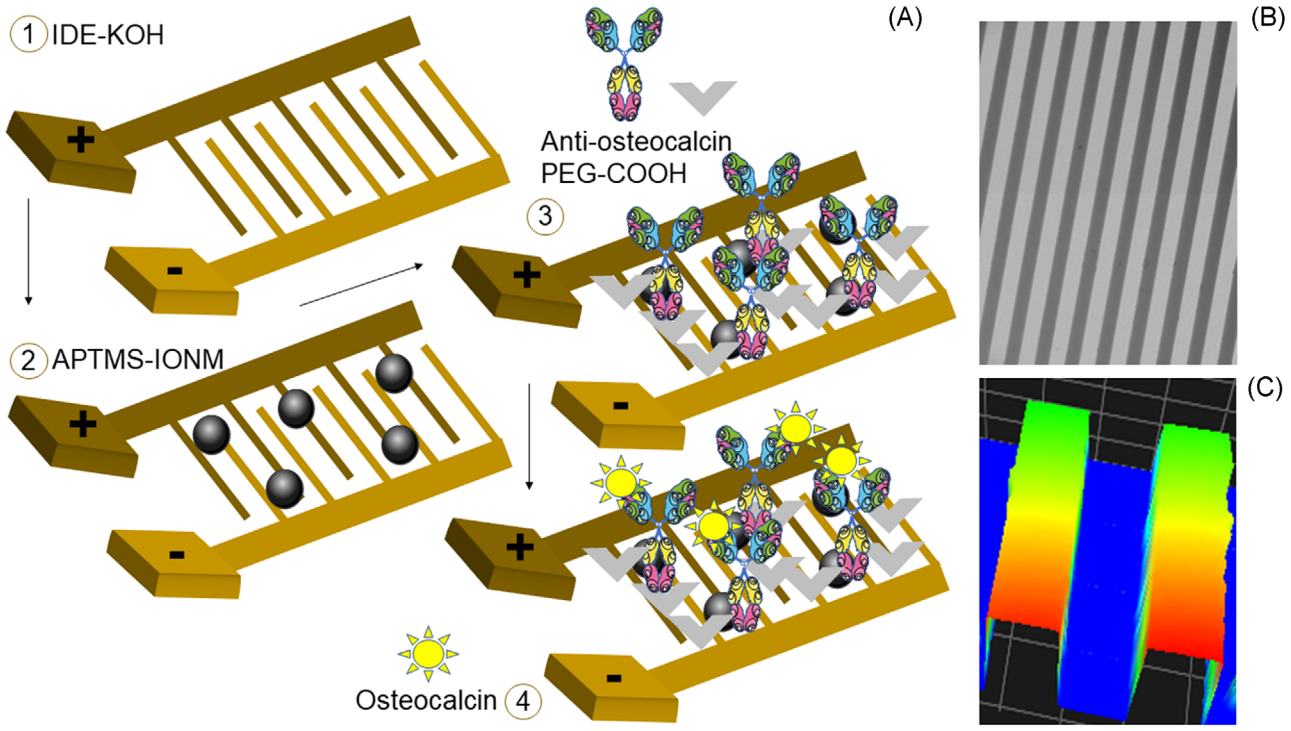

FIGURE 2 (A) Schematic of osteocalcin detection on iron oxide material (IOM)-modified electrode. Surface of electrode was modified with APTMS-IOM and then antiosteocalcin antibody was immobilized. Antibody-attached surface used to identify the osteocalcin level after blocking by PEG-COOH. (B) High-power microscope image of electrode surface. (C) Electrode surface under 3D-nanopiling imager. Clear discriminating patterns are seen as gap and finger regions

APTMS-IONW-modified electrode and rested (for 1 h), followed by washing steps with PBS buffer. On these antibody-coated electrode surfaces, osteocalcin was detected.

2.6 | Osteocalcin identification on antibody-attached surface

Osteocalcin and its antibody binding affinity on IDE electrode surface were measured by changing the current/volt upon binding of osteocalcin. Before this process, the excess surface of antibody-modified electrode was covered by 1 mg/ml PEG-COOH. And then osteocalcin concentrations (10 pg/ml to 4 μg/ml) were diluted in PBS and allowed to immobilize the antibody. The current change for each experiment was recorded. The difference in current was calculated and plotted to calculate the detection limit of osteocalcin.

2.7 | Specific osteocalcin detection

For the selective osteocalcin process, control proteins, such as albumin, globulin, and nonimmune antibodies, were utilized. Instead of osteocalcin, albumin and globulin were dropped individually on antiosteocalcin-modified electrode surface and then the current response was recorded. In another experiment, nonimmune antibody was modified on the electrode surface and then osteocalcin was interacted. The current response was compared with the specific osteocalcin identification. Unless otherwise stated, sensor operates on the dual-probe station with the current-volt supply at the range of 0–2 V, with an interval of 0.1 V. The operating conditions were kept wet throughout the experiments by using 10 mM PBS (pH 7.4) at room temperature. Thorough washings were performed between the immobilization steps/surface modifications. Triplicate experiments were followed and the values were averaged.

3 | RESULTS AND DISCUSSION

3.1 | Characterization and functionalization of electrode surface

Figure 2A shows the schematic diagram of osteocalcin quantification on IOM-modified interdigitated electrode surface. As shown in the figure, surface of IDE was treated with KOH, and then APTMS-IOM was modified on the surface. Further, antiosteocalcin was dropped on the surface to allow the interaction of COOH in the antibody with NH_2 of the APTMS surface. And then, the excess APTMS

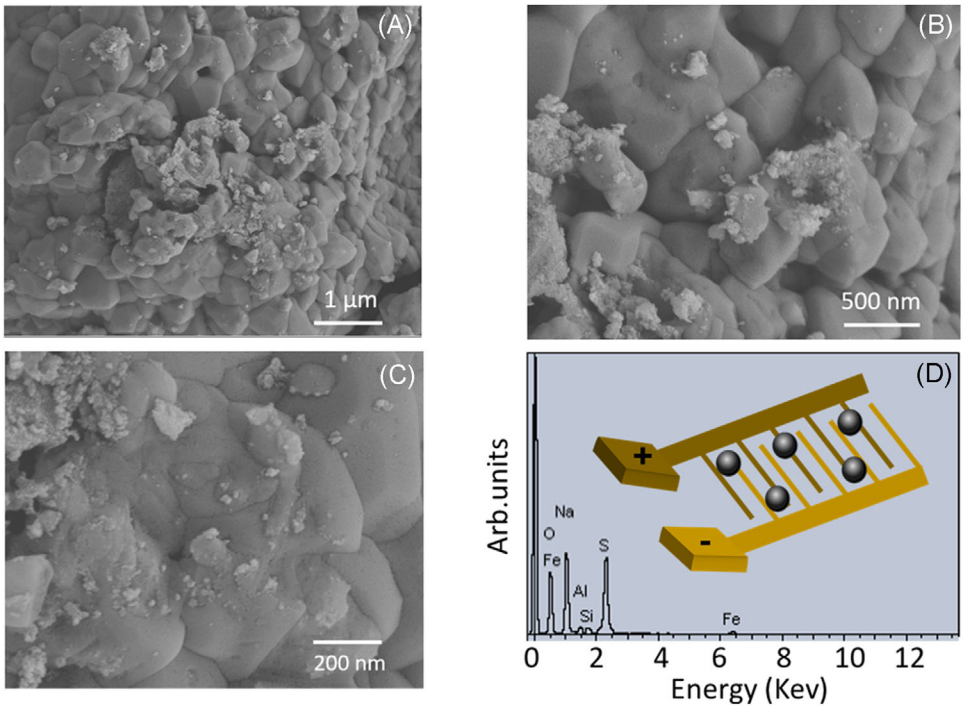

FIGURE 3 FESEM image of iron oxide material (IOM) with the scale of (A) 1 μm; (B) 500 nm; and (C) 200 nm. (D) EDX analysis of IOM. EDX result confirms the presence of iron in the synthesized material. Figure inset displays the sensing surface

was blocked with PEG-COOH. Here PEG-COOH was utilized for blocking agent as well as used for aligning the immobilized antibody properly. Various research studies proved that PEG-based polymers drastically reduced the biofouling attachment on the sensing electrode and provide the proper arrangement of the immobilized capture molecule.[29] This aids in lowering the limit of detection of target molecule. This antibody-attached surface aids in identifying the osteocalcin at its lower level.

Before performing the surface modification, the intactness of the surface electrodes was attested by 3D nanoprofiler and high-power microscope (Figure 2B,C). IOM was extracted and synthesized from the coal fly ash. The surface morphology of IOM was imaged by FESEM. Figure 3A–C displays the FESEM image of IOM at different scales. The iron materials are tightly backed with uniform shape and multifaceted as bulky. The EDX result conforms the presence of iron in the synthesized material (Figure 3D).

3.2 | Capture antibody immobilization on IOM-modified electrode surface

Antiosteocalcin antibody immobilization on the IOM surface was monitored by measuring the changes in the current after introducing each biomolecule on the electrode surface. As in Figure 4A, bare electrode displays the current level as 1.04×10^{-8} A, after APTMS-IOM attaches on the surface, the current was changed to 8.84×10^{-7} A. And when antibody was introduced, the current was elevated drastically to 4.24×10^{-6} A, which confirmed the antibody immobilization on the IDE electrode surface. As several APTMS molecules were attached on a single IONW, it attracted higher number of antibodies on the sensing electrodes surface, which in turn helps to reduce the detection limit of osteocalcin (Figure 4B). Finally, the uncovered electrode surface was masked by the blocking agent PEG-COOH, which helped to reduce the signal-to-noise ratio and elevate the sensitivity.

3.3 | Osteocalcin determination on IDE electrode

Osteocalcin was identified by its antibody on IONW-modified surface. Osteocalcin concentrations from 10 pg/ml to 4 μg/ml were dropped individually on antibody-attached electrode surface and then the current responses were recorded. PEG-COOH-blocked electrode surface displayed the current level as 6.58×10^{-6} A, and after 10 pg/ml of osteocalcin was dropped, there was no significant change of current noticed (Figure 5A). And then increasing the osteocalcin concentration to 100 pg/ml, the current was elevated to 7.5×10^{-6} A. On further increment in osteocalcin concentrations to

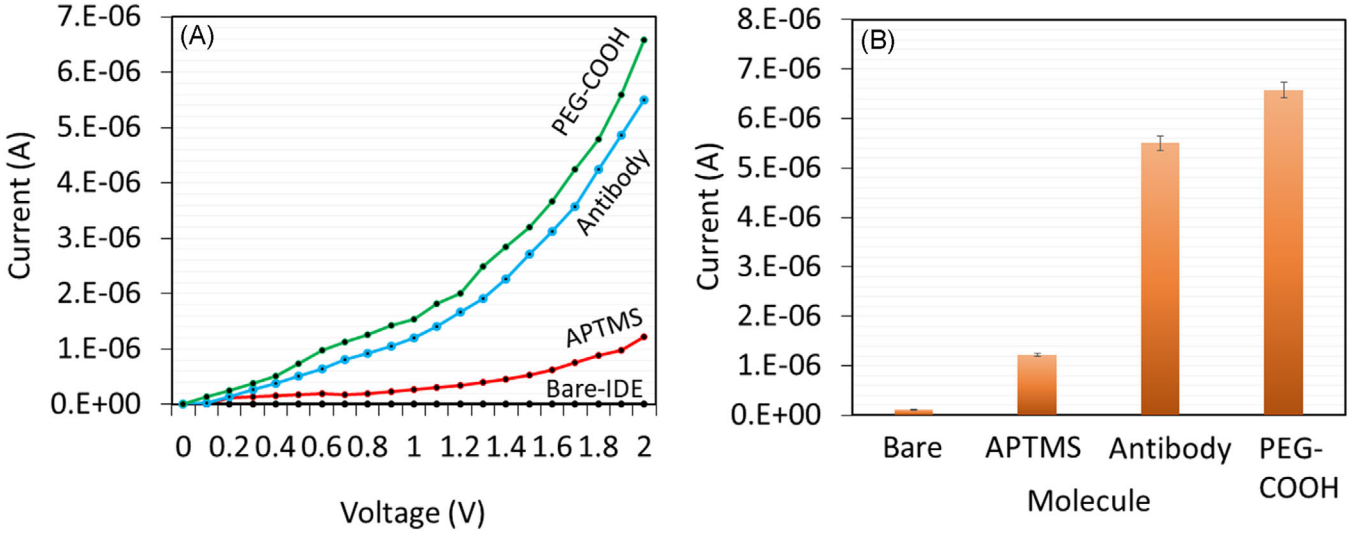

FIGURE 4 (A) Antiosteocalcin antibody immobilization on iron oxide material (IOM). Current response was clearly increased after each immobilization step. (B) Current levels with antibody immobilization process. After antibody attachment, higher response of current was noted. Data were averaged by triplicates

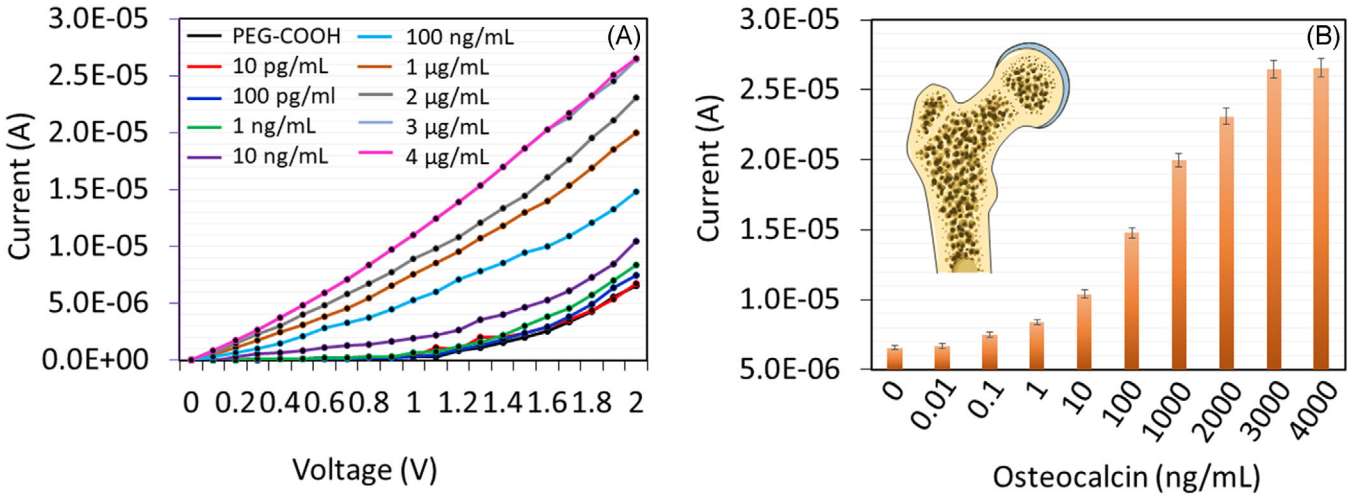

FIGURE 5 (A) Osteocalcin was detected by its antibody on iron oxide material (IOM)-modified electrode. Osteocalcin concentrations from 10 pg/ml to 4 μg/ml were made to interacte with antibodies. From 100 pg/ml, current response was increased. (B) Current response for different concentrations of osteocalcin interaction with antibody. Increasing osteocalcin concentrations were responded with current increment gradually. Further, the interaction of osteocalcin with antibody was saturated at 2 μg/ml. Data were averaged by triplicates. Figure inset shows the osteoporosis of bone

1, 10, 100, 1000, 2000, 3000, and 4000 ng/ml, current responses were increased to 8.4×10^{-6}, 1.04×10^{-5}, 1.48×10^{-5}, 2.0×10^{-5}, 2.31×10^{-5}, 2.65×10^{-5}, and 2.66×10^{-5} A, respectively. It was identified that with enhancing osteocalcin, the response of current was also elevated gradually. Further, it was noticed that the interaction of osteocalcin with its antibody was saturated at 3 μg/ml, indicating attainment of the maximum detection level (Figure 5B). The difference in current response for each osteocalcin concentration was calculated and plotted and it was found that the detection limit of osteocalcin was 100 pg/ml with the R^2 value of 0.9319 (Figure 6A).

3.4 | Specific osteocalcin detection

Specific osteocalcin interaction with its antibody was confirmed by various control experiments. Control

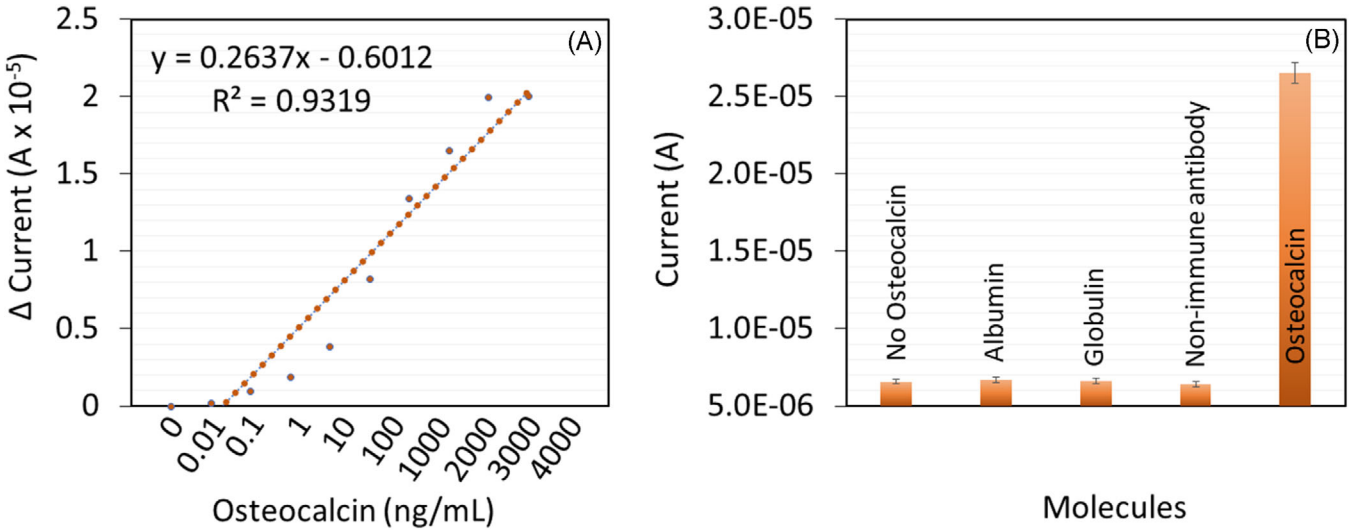

FIGURE 6 (A) Difference of current response for each osteocalcin concentration. Calculated and plotted in an excel sheet, and found the detection limit of osteocalcin as 100 pg/ml with R^2 value of 0.9319. (B) Specific osteocalcin interaction with antibody. No significant current responses are noted with control molecules, indicating the specific identification of osteocalcin on IONW-modified electrode surface

experiment was conducted using albumin, globulin, and nonimmune antibody. To connect the clinical relevancy, the major proteins in human serum, such as albumin and globulin, were desired as control proteins to analyze the interference. Albumin and globulin are in the human serum at the levels of 3.5–5.0 and 2.6–3.5 g/dl, respectively. Figure 6B clearly indicates that there is no significant current response with control experiments, even when present in abundance, indicating the specific identification of osteocalcin on IONW-modified IDE electrode.

4 | CONCLUSION

Osteoporosis is the condition of bone tissue deterioration, causing the risk of weakened bones and bone fractures. Identifying osteoporosis at its earlier stage helps to recover the original bone condition. Osteocalcin is identified as the suitable biomarker for early identification of osteoporosis. This research was focused to quantify osteocalcin by its antibody on interdigitated electrode surface. Silane-modified IOM was utilized to attach antiosteocalcin on the electrode surface. On this antibody-modified electrode, the limit of detection of osteocalcin reached 100 pg/ml. Further, experiments with control proteins failed to bind with immobilized antibody, confirming the specific osteocalcin detection. This research work was to identify the osteoporosis biomarker and to help monitor the condition of osteoporosis. The critical point needs to be considered with this sensor is optimization on the surface when different nanomaterial is used. In addition, the limitation with micro-electrode gaps is that the system gets short circuit when the gaps are minimized to nano-range.

ACKNOWLEDGMENTS

Thanks to the Servier Medical Art for reproducing their images.

ORCID

Subash C. B. Gopinath https://orcid.org/0000-0002-8347-4687

Genbing Lv https://orcid.org/0000-0001-5257-0820

REFERENCES

1. Inal Kabala S, Yagar H, Ozcan HM. A new biosensor for osteoporosis detection. Prep Biochem Biotechnol. 2019;49:511–20.
2. Afsarimanesh N, Alahi MEE, Mukhopadhyay SC, Kruger M. Smart sensing system for early detection of bone loss: current status and future possibilities. J Sens Actuator Netw. 2018;7:10.
3. Srivastava RK, Dar HY, Mishra PK. Immunoporosis: immunology of osteoporosis-role of T cells. Front Immunol. 2018;9:657.
4. Rani S, Bandyopadhyay-Ghosh S, Ghosh SB, Liu G. Advances in sensing technologies for monitoring of bone health. Biosensors. 2020;10:42.
5. Khashayar P, Amoabediny G, Larijani B, Vanfleteren J. Bone biosensors: knowing the present and predicting the future. J Micromech Microeng. 2016;26:23002.
6. Vohra M, Sharma A, Bagga R, Arora SK. Human umbilical cord derived mesenchymal stem cells induce tissue repair and regeneration in collagen-induced arthritis in rats. J Clin Transl Res. 2020;6:203–16.
7. Bai H, Chen G, Fang C, Yang X, Yu S, Hai C. Osteosarcoma cell proliferation and migration are partly regulated by redox-activated NHE-1. J Clin Transl Res. 2015;1:168–79.

8. Singh P, Shrivastava A. Optical biosensor based on microbendings technique: an optimized mean to measure the bone strength. Adv Opt Technol. 2014;2014:853725.
9. Afsarimanesh N, Mukhopadhyay SC, Kruger M. Sensing technologies for monitoring of bone-health: a review. Sens Actuator A Phys. 2018;274:165–78.
10. Mcgill MR, Jaeschke H. Biomarkers of mitotoxicity after acute liver injury: further insights into the interpretation of glutamate dehydrogenase. J Clin Transl Res. 2021;7:61–5.
11. Montano N. Biomarkers in glioblastoma multiforme. Evidences from a literature review. J Clin Transl Res. 2016;2:3–10.
12. Moser SC, van der Eerden BCJ. Osteocalcin — a versatile bone-derived hormone. Front Endocrinol (Lausanne). 2019;10:794.
13. Zoch ML, Clemens TL, Riddle RC. New insights into the biology of osteocalcin. Bone. 2016;82:42–9.
14. Singh S, Kumar D, Lal AK. Serum osteocalcin as a diagnostic biomarker for primary osteoporosis in women. J Clin Diagn Res. 2015;9:RC04–7.
15. Zhao J, Chang W, Liu L, Xing X, Zhang C, Meng H, et al. Graphene oxide-gold nanoparticle-aptamer complexed probe for detecting amyloid beta oligomer by ELISA-based immunoassay. J Immunol Methods. 2021;489:112942.
16. Ibau C, Arshad MKM, Gopinath SCB, Nuzaihan M, Fathil MFM, Shamsuddin SA. Immunosensing prostate-specific antigen: Faradaic vs non-Faradaic electrochemical impedance spectroscopy analysis on interdigitated microelectrode device. Int J Biol Macromol, 2020;162:1924–36.
17. Yao J, Li S, Zhang L, Yang Y, Gopinath SCB, Lakshmipriya T, et al. Aptamer-antibody dual probes on single-walled carbon nanotube bridged dielectrode: comparative analysis on human blood clotting factor. Int J Biol Macromol. 2020;151:1133–8.
18. Carrasco-esteban E, Domínguez-rullán JA, Barrionuevo-castillo P, Pelari-mici L, López-campos F. Current role of nanoparticles in the treatment of lung cancer. J Clin Transl Res. 2021;7:140–55.
19. Chen S, Jang TS, Pan HM, Jung HD, Sia MW, Xie S, et al. 3D freeform printing of nanocomposite hydrogels through in situ precipitation in reactive viscous fluid. Int J Bioprint. 2020;6:258.
20. Ramanathan S, Gopinath SCB, Arshad MKM, Poopalan P. Nanostructured aluminosilicate from fly ash: potential approach in waste utilization for industrial and medical applications. J Clean Prod. 2020;253:119923.
21. Ding Y, Tian Q, Dong Y, Xing L, Gopinath SCB, Mao Y. Gold-silane complexed antibody immobilization on polystyrene ELISA surface for enhanced determination of matrix metalloproteinase-9. Process Biochem. 2021;100:231–6.
22. Wang Y, Guo Y, Lu J, Sun Y, Yu X, Gopinath SCB, et al. Nanodetection of head and neck cancer on titanium oxide sensing surface. Nanoscale Res Lett. 2020;15:33.
23. Shuai C, Li Y, Yang W, Yu L, Yang Y, Peng S, et al. Graphene oxide induces ester bonds hydrolysis of poly-l-lactic acid scaffold to accelerate degradation. Int J Bioprint. 2020;6:91–104.
24. Rueda-Gensini L, Serna JA, Cifuentes J, Cruz JC, Muñoz-Camargo C. Graphene oxide-embedded extracellular matrix-derived hydrogel as a multiresponsive platform for 3D bioprinting applications. Int J Bioprint. 2021;7:353.
25. Hou Y, Wang W, Bártolo P. Investigating the effect of carbon nanomaterials reinforcing poly(ε-caprolactone) printed scaffolds for bone repair applications. Int J Bioprint. 2020;6:266.
26. Zhang Y, Attarilar S, Wang L, Lu W, Yang J, Fu Y. A review on design and mechanical properties of additively manufactured NiTi implants for orthopedic applications. Int J Bioprint. 2021;7:340.
27. Hong X, Hong X, Zhao H, Chen C, Gopinath SCB, Daniel L, et al. Improved immunoassay for insulin-like growth factor 1 detection by aminated silica nanoparticle in ELISA. Process Biochem. 2020;91:282–7.
28. Zhang J, Gopinath SCB. Quantification of cortisol for the medical diagnosis of multiple pregnancy-related diseases. 3 Biotech. 2020;10:35.
29. Lakshmipriya T, Fujimaki M, Gopinath SCB, Awazu K, Horiguchi Y, Nagasaki Y, et al. A high-performance waveguide-mode biosensor for detection of factor IX using PEG-based blocking agents to suppress non-specific binding and improve sensitivity. Analyst. 2013;138:2863.

How to cite this article: Bi H, Bian P, Gopinath SCB, Marimuthu K, Lv G, Yin XH. Identifying mineral decrement with bone injury by quantifying osteocalcin on current-volt sensor. Biotechnology and Applied Biochemistry. 2022;69:2061–2068. https://doi.org/10.1002/bab.2267